Hu et al. Nanoscale Research Letters (2017) 12:435
DOI 10.1186/s11671-017-2204-8

Nanoscale Research Letters

NANO EXPRESS Open Access

One-Pot Green Synthesis of Ag-Decorated SnO_2 Microsphere: an Efficient and Reusable Catalyst for Reduction of 4-Nitrophenol

Min Hu, Zhenwei Zhang, Chenkun Luo and Xiuqing Qiao*

Abstract

In this paper, hierarchical Ag-decorated SnO_2 microspheres were synthesized by a facile one-pot hydrothermal method. The resulting composites were characterized by XRD, SEM, TEM, XPS, BET, and FTIR analysis. The catalytic performances of the samples were evaluated with the reduction of 4-nitrophenol to 4-aminophenol by potassium borohydride (KBH_4) as a model reaction. Time-dependent experiments indicated that the hierarchical microspheres assembled from SnO_2 and Ag nanoparticles can be formed when the react time is less than 10 h. With the increase of hydrothermal time, SnO_2 nanoparticles will self-assemble into SnO_2 nanosheets and Ag nanoparticles decorated SnO_2 nanosheets were obtained. When evaluated as catalyst, the obtained Ag-decorated SnO_2 microsphere prepared for 36 h exhibited excellent catalytic performance with normalized rate constant (κ_{nor}) of 6.20 $min^{-1}g^{-1}L$, which is much better than that of some previous reported catalysts. Moreover, this Ag-decorated SnO_2 microsphere demonstrates good reusability after the first five cycles. In addition, we speculate the formation mechanism of the hierarchical Ag-decorated SnO_2 microsphere and discussed the possible origin of the excellent catalytic activity.

Keywords: Ag-decorated SnO_2, Microsphere, Hydrothermal, Catalytic, 4-Nitrophenol, Hierarchical

Background

SnO_2 is an important n-type semiconductor with large bandgap (Eg = 3.6 eV, at 300 K), high electron mobility, and low cost, which enable it with outstanding properties in gas sensing [1], lithium ion batteries [2], optoelectronic devices, and dye sensitized solar cells [3–8]. In the past two decades, the robust SnO_2 material has garnered considerable attention and various nanostructures have been reported [9, 10]. Among which, three-dimensional (3D) hierarchical structures self-assembled by nanosheets building blocks are much more interesting due to their special structure and fascinating properties [11, 12]. Nevertheless, there are only a few reports on the catalytic performance of SnO_2 and the catalytic efficiency is relatively low [13–15]. It is thus important to synthesize hierarchical SnO_2 structures and study the catalytic performance. Especially, as we know, noble metal nanoparticles (NPs) such as Au-, Ag-, Pt-, and Pd-modified 3D hierarchical structures will show much enhanced catalytic performance [16]. However, most of the processes of the syntheses of the above noble metal-modified oxides are more complicated multi-step process and usually toxic and harmful environmentally [17]. So developing facile and efficient methods to fabricate noble metal NP-modified hierarchical SnO_2 and studying the catalytic performance are highly desirable.

Increased contamination of our limited water resources owing to the widespread dispersion of various industrial dyes, heavy metal ions, and other aromatic pollutants are endangering our planet [18]. The 4-nitrophenol (4-NP), a well-known toxic pollutant, is widely present in industrial effluents and agriculture wastewater [19]. Among various treatment techniques, such as membrane filtration [20], photo degradation [21], adsorption [22], and chemical reduction [23–30], the chemical reduction of 4-NP to 4-aminophenol (4-AP) is a favorable route, owing to the

* Correspondence: 280186517@qq.com
College of Materials and Chemical Engineering, Hubei Provincial Collaborative Innovation Center for New Energy Microgrid, Key Laboratory of Inorganic Nonmetallic Crystalline and Energy Conversion Materials, China Three Gorges University, Yichang 443002, Hubei, People's Republic of China

product (4-AP) which is an important intermediate for the manufacture of analgesic and antipyretic drugs, photographic developer, corrosion inhibitor, anticorrosion lubricant, and hair-dyeing agent [31, 32]. Hence, the reduction of 4-NP to 4-AP possesses great significance for the pollution abatement and resource regeneration [33].

In this paper, we reported a green synthesis of noble metal Ag nanoparticle (NP)-modified SnO_2 hierarchical architectures by a simple one-pot hydrothermal route without the assistant of any templates and surfactants at mild temperature. The effects of reaction time on morphologies of Ag-decorated SnO_2 microsphere were investigated, and a possible growth mechanism of Ag-decorated SnO_2 hierarchical structures was proposed. The catalytic results indicate the as-synthesized products exhibit excellent catalytic performance for the reduction of 4-NP to 4-AP, with normalized rate constant (κ_{nor}) of 6.20 $min^{-1}g^{-1}L$. In addition, the Ag-decorated SnO_2 hierarchical structures sustain high catalytic efficiency in ten cycles and show stability after the first five cycles. This obtained Ag-decorated SnO_2 hierarchical structures may have potential applications of water contaminant treatment, and this simple one-step hydrothermal route could be extended to design other noble metal NP-modified composite with a wide range of practical applications for the future.

Methods

Materials

Silver nitrate ($AgNO_3$, 99.8%), urea ($CO(NH_2)_2$, 99%), ammonia solution ($NH_3{\cdot}H_2O$, 25~28%), and potassium borohydride (KBH_4, 97%) were purchased from Sinopharm Chemical Reagent Co. Ltd. Sodium stannate rehydrate ($Na_2SnO_3{\cdot}3H_2O$, 98%) and 4-nitrophenol($C_6H_5NO_3$, 98%) were supplied by Aladdin Reagent Co. Ltd. All the materials were used without further purification.

Synthesis of Ag-Decorated SnO_2 Microsphere

Ag-decorated SnO_2 powder (mole ratio of Ag:SnO_2 = 1:1) was synthesized by one-pot hydrothermal method. In a typical procedure, 2.67 g of sodium stannate rehydrates and 0.2 g of urea were dissolved in 25 mL of ultra-pure water and stirred vigorously for 30 min to form a mixture. Then, 1.69 g of silver nitrate was dispersed in 25 mL of ultra-pure water, and then, 2.4 mL ammonium hydroxide was added into the silver nitrate solution to form silver–ammonia solution. After stirring for 5 min, the freshly prepared silver–ammonia solution was added into the mixture under magnetic stirring for 1 h. Subsequently, the resulting mixture was migrated into a 50-mL Teflon-lined autoclave and heated at 150 °C for 5, 10, 24, and 36 h. After the hydrothermal procedure, the autoclave was cooled down naturally to room temperature and the SnO_2/Ag product was collected by centrifugation, followed by rinsing with deionized water and ethanol and drying in a vacuum oven at 60 °C. SnO_2/Ag microsphere with different mole ratios (1.5:1, 1:1, 0.5:1, 0.01:1) of Ag to SnO_2 are synthesized in a similar way except for the amounts of $AgNO_3$ and $NH_3{\cdot}H_2O$. For comparison, pure SnO_2 and Ag were also synthesized by the similar procedure without the addition of $AgNO_3$ and Na_2SnO_3.

Sample Characterizations

The crystalline phase of the as-prepared samples were investigated by X-ray powder diffraction (XRD, Cu Kα radiation (λ = 1.5418 Å)). The scanning electron microscopy (SEM) measurements were performed on a SU-70 field emission SEM microscope with an acceleration voltage of 20 kV. Transmission electron micrograph (TEM) and high-resolution transmission electron microscopy (HRTEM) were taken on a Tecnai G2 F20 S-TWIN transmission electron microscope with an accelerating voltage of 200 kV. X-ray photo-electron spectroscopy (XPS) was performed to identify surface chemical composition and chemical states of the catalysts on a MARK II X-ray photoelectron spectrometer using Mg Kα radiation. The specific surface area of sample was evaluated by the Langmuir model and Brunauer–Emmett–Teller (BET) model based on the nitrogen adsorption isotherm obtained with a V-sorb X2008 series, while the pore size distribution was estimated by Barrett–Joyner–Halenda (BJH) theory.

Catalytic Activity of Ag-Decorated SnO_2 Microsphere

The reduction of 4-NP with KBH_4 solution was used as a model reaction to study the catalytic activity of Ag-decorated SnO_2 composites. The catalytic reduction process was carried out in a standard quartz cell with a 1-cm path length and about 4 mL volume with 0.3 mL of freshly prepared aqueous solutions of 4-NP (20 mg/L) and KBH_4 (1.5 mg). The high molar ratio of KBH_4 to 4-NP ensured an excess amount of the former, and hence, its concentration remained essentially constant during the reduction reaction. Upon the addition of KBH_4 into the 4-NP solution, its color changed immediately from light yellow to dark yellow due to the formation of 4-nitrophenolate ion (formed from the high alkalinity of KBH_4). Later, the dark yellow color faded with time (due to the conversion of 4-NP to 4-AP) after the addition of 1.5 mg of Ag-decorated SnO_2 hybrids. The UV–Vis absorption spectra were recorded by an UV–Vis spectrometer in a scanning range of 250–500 nm at room temperature at time interval of 1 min. Several consecutive reaction rounds were measured to determine the stability of the catalyst.

Results and Discussion

Characterization of Ag-Decorated SnO_2 Microsphere

The composition and phase structure of the synthesized Ag-decorated SnO_2 powders for different times were investigated by XRD, and the corresponding patterns are shown

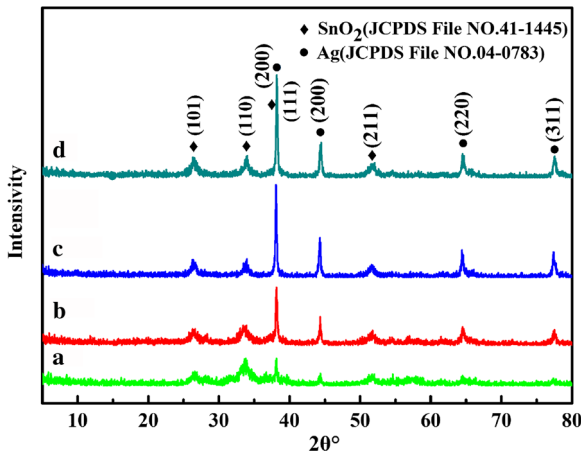

Fig. 1 XRD patterns of the Ag-decorated SnO_2 microspheres prepared at 150 °C for different times (*a*) 5 h, (*b*) 10 h, (*c*) 24 h, and (*d*) 36 h

in Fig. 1. It can be seen that the characteristic diffraction peaks match well with the tetragonal rutile phase SnO_2 (JCPDS file no. 41-1445, $a = 4.738$Å and $c = 3.187$ Å) and face centered cubic (fcc) phase Ag (JCPDS file no. 04-0783). No diffraction peaks from any other impurities were detected indicating that the powders are the mixture of pure SnO_2 and Ag. For the sample reacted for 5 h, the characteristic diffraction peaks at 38.12° and 44.2°, corresponding to the (111) and (200) planes of Ag, are relatively weak. With increasing hydrothermal time, the peak intensities of Ag increase and the full widths of diffraction peak decrease as well, indicating the enhanced crystallinity of Ag nanoparticles or the increased weight of Ag. This can be further verified by the XRD patterns of the samples obtained under different temperatures and different mole ratios of Ag and SnO_2 (Additional file 1: Figure S1).

The SEM images in Fig. 2 show the interesting morphological evolution of samples prepared at different hydrothermal times from 5 to 36 h. Sample prepared for 5 h was irregular microsphere, and the enlarged view of the surface of microspheres in the inset illustrating the microsphere is assembled by nanoparticles (Fig. 2a). With increasing

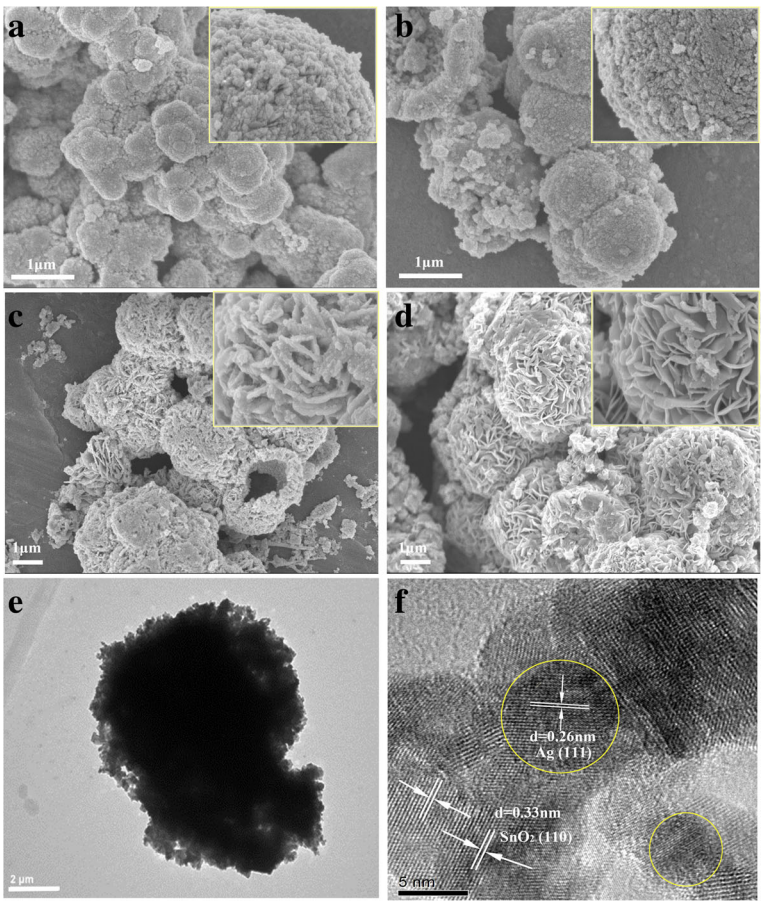

Fig. 2 Representative FESEM images and TEM images of the Ag-decorated SnO_2 microspheres prepared at 150 °C for different hydrothermal times **a** 5h, **b** 10h, **c** 24h, and **d** 36h and **e**, **f** low-magnification TEM image and high-resolution TEM (HRTEM) of the sample prepared for 36 h

hydrothermal time, the microsphere became more regular. Upon the hydrothermal time increased to 24 h (Fig. 2c), the microsphere grew larger at the expense of the smaller nanoparticles and the surface nanoparticles self-assembled into nanosheets. These nanosheets assembled to form a hierarchical microsphere structure. When further increasing the hydrothermal time to 36 h, the coarse nanosheets became smoothed and the microspheres with diameters ranging from 2 to 4 μm are more uniform. Further increase of the hydrothermal time led no obvious change of the morphology and crystalline (not shown in this paper). The morphology of the sample prepared for 36 h was further observed via TEM and HRTEM. As shown in Fig. 2e, the obtained SnO_2/Ag is of microsphere morphology with diameter of ~5 μm and the microsphere is assembled from nanosheets. In the typical HRTEM image (Fig. 2f), Ag NPs with an average size of about 5 nm were formed and homogeneously distributed to SnO_2. The lattice fringes of $d = 0.26$ nm spacing can be assigned to the Ag (111) planes while the lattice fringes of $d = 0.33$ nm can be assigned to the (110) plane of SnO_2, respectively. To further illustrate the uniform distributions of Ag nanoparticles in the microsphere, element mapping analysis of the SnO_2/Ag microsphere was performed (Fig. 3). As shown in the Fig. 3, the map of Ag, Sn, and O elements are fit into the sample morphology, indicating that Ag nanoparticles are uniformly dispersed in the microspheres.

The N_2 adsorption–desorption isotherms of samples and their corresponding pore size distribution are illustrated in Fig. 4. All of the samples exhibited type IV isotherms with H_3 hysteresis loop, signifying typical mesoporous structures of uniform pore size [34]. The BET-specific surface areas were determined as 21.8, 22.4, 24.6. and 25.7 $m^2\ g^{-1}$, respectively. Inset depicts the pore size distributions of samples. The pore size distribution is mono-modal for all the samples. The average pore diameter is ~2 nm for the as-hierarchical Ag-decorated SnO_2 powders. It is noted that the calculated BET surface area and mean pore diameter has no obvious change with increasing hydrothermal time.

XPS was used to examine the chemical states and surface composition of Ag-decorated SnO_2 microspheres. Wide survey scans were recorded first followed by a detailed scanning of the edges of each element such as Sn 3d, Ag 3d, and O 1s (Fig. 5). It may be mentioned that the charging effect on the sample was corrected by setting the binding energy of the carbon (C 1s) at 284.6 eV and this carbon peak was used as a reference position for scaling all other peaks. As shown in Fig. 5b, the peak appears as a spin–orbit doublet at 369.1 eV (Ag $3d_{5/2}$) and 375.2 eV (Ag $3d_{3/2}$) for Ag^0 [35, 36] in the product. The two satellite peaks at 366.5 and 372.3 eV can be account for Ag 3d in Ag-decorated SnO_2 nanocomposites [37]. Furthermore, two XPS peaks located at 488 and 496.7 eV are relevant to Sn $3d_{5/2}$ and Sn $3d_{3/2}$, indicating the presence of Sn^{4+} in SnO_2. And the peaks around 485.7 and 494.7 eV may be caused by the binding between Sn and Ag [38, 39]. The slightly binding energy

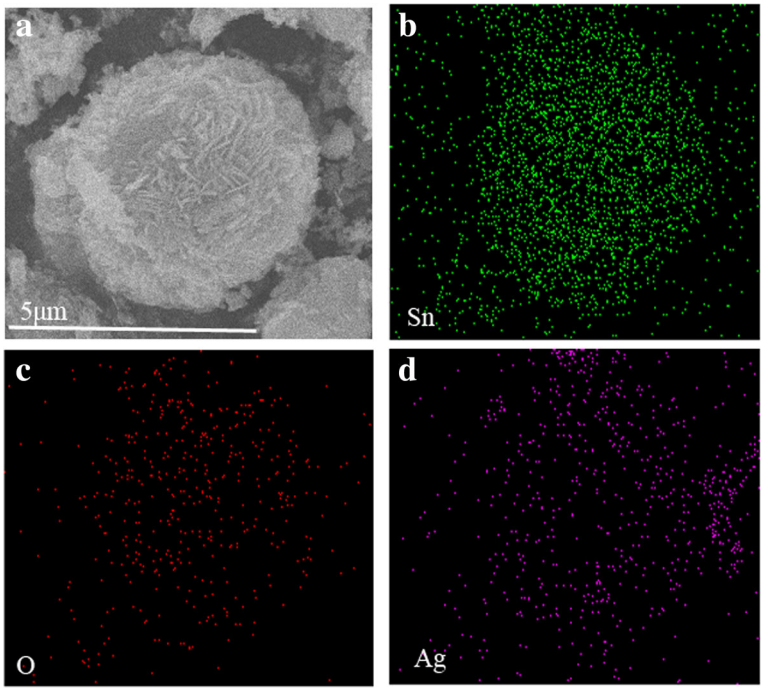

Fig. 3 EDS element mapping of SnO_2/Ag microspheres. **a** SEM image and element maps of **b** Sn, **c** O, and **d** Ag

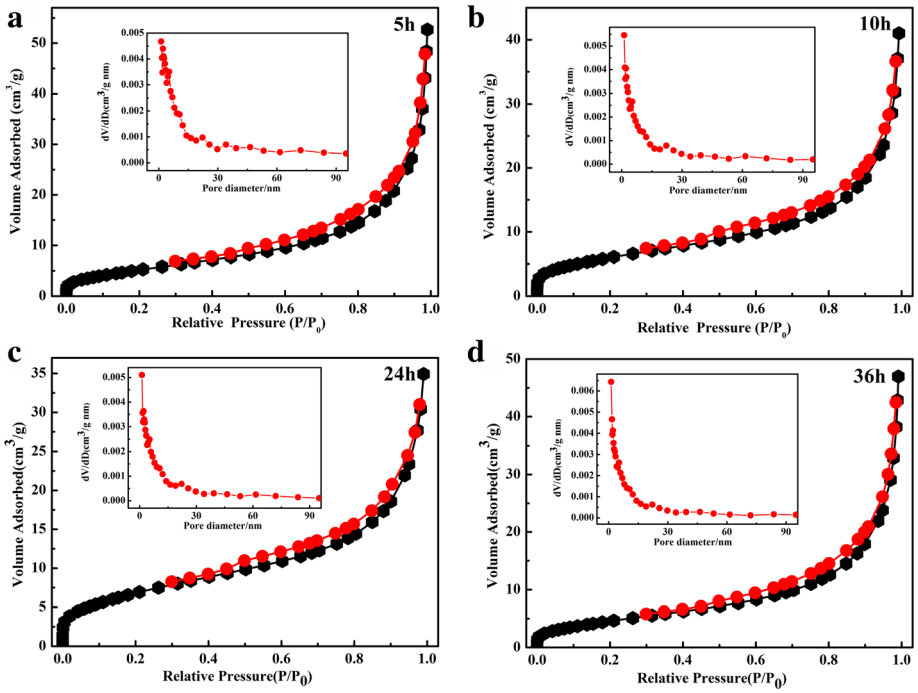

Fig. 4 Typical nitrogen adsorption–desorption isotherm of the prepared SnO_2/Ag microspheres prepared at 150 °C for different hydrothermal times **a** 5 h, **b** 10 h, **c** 24 h, and **d** 36 h

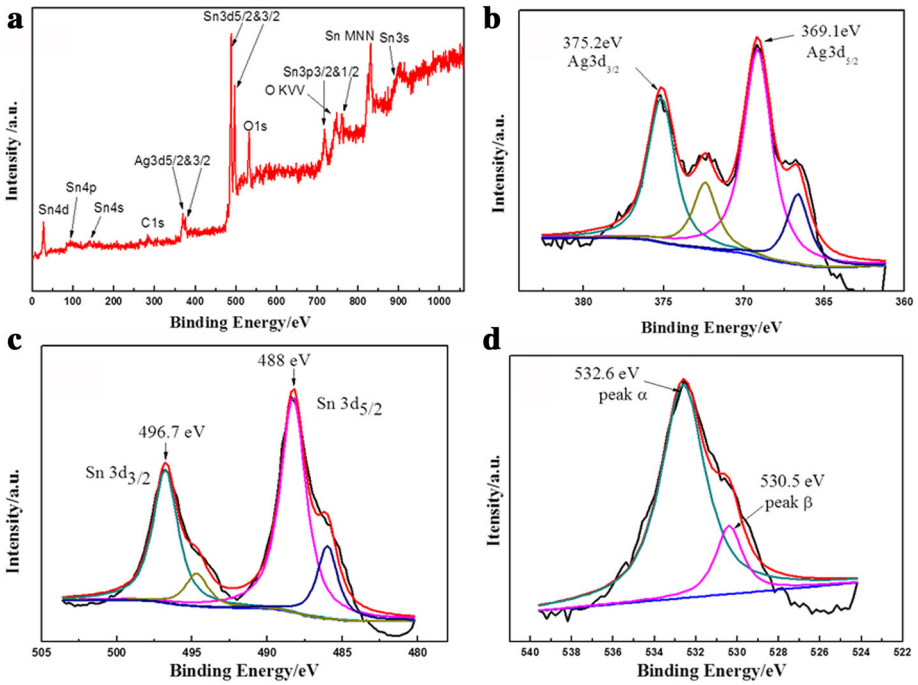

Fig. 5 Representative XPS spectra of SnO_2/Ag microspheres prepared at 150 °C for 36 h. **a** XPS full spectra. High-resolution spectra of the elements **b** Ag, **c** Sn, and **d** O

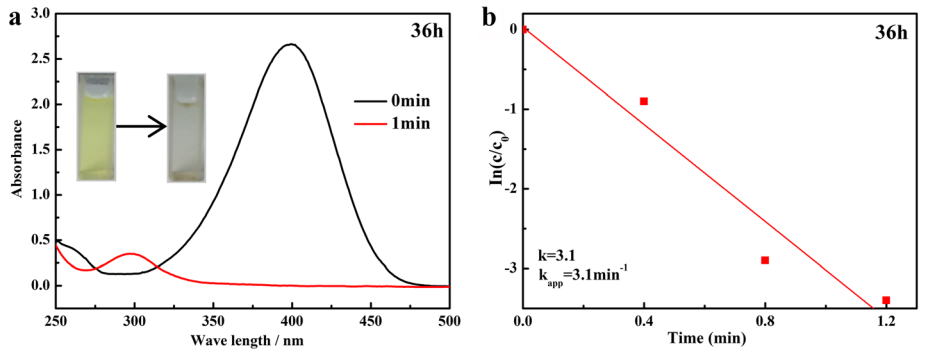

Fig. 6 **a**, **b** Time-dependent UV–Vis absorption spectra and the plot of $\ln(C_t/C_0)$ versus reaction time for the reduction of 4-NP of the sample prepared at 150 °C for 36 h

shift of these elements in Ag-decorated SnO_2 microsphere means electrons may transfer between Ag and SnO_2, demonstrating strong interaction between Ag nanoparticles and SnO_2 nanosheets rather than simply physical contact. The strong interaction is advantageous for the electron transfer among the adjacent particles, which can improve the catalytic activities and be beneficial to some similar phenomenon, which was observed in other literatures [38–40]. In Fig. 5d, O 1s spectra at 530.5 eV corresponded to the lattice oxygen while the peak at 532.6 eV corresponds to chemisorbed oxygen or hydroxyl ions such as O^-, O_2^-, or OH^- at the surface of SnO_2 [41–44].

Catalytic Reduction of 4-NP

The reduction of 4-NP by KBH_4 in the presence of catalyst is a well-studied green chemical reaction and was chosen as the model reaction to study the catalytic activity of the as-prepared Ag-decorated SnO_2 composites. The UV–Vis absorption spectrum with a maximum absorption at 400 nm is formed due to the nitro compound. With the Ag-decorated SnO_2 catalyst added, the absorption peak at 400 nm, ascribed to nitro compounds, decreased sharply in 1 min and a new peak at 300 nm corresponding to 4-AP appeared, indicating the catalytic reduction of 4-NP had proceeded successfully (Fig. 6a). Considering of the

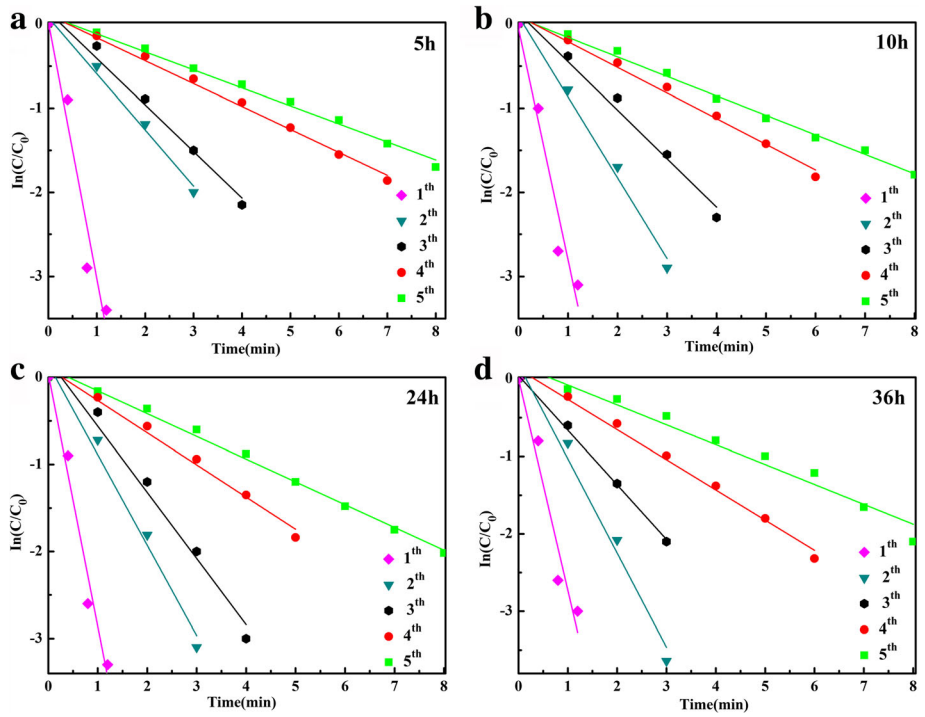

Fig. 7 Plot of $\ln(C_t/C_0)$ versus reaction time in the presence of Ag-decorated SnO_2 microspheres prepared for different hydrothermal times **a** 5 h, **b** 10 h, **c** 24 h, and **d** 36 h

Table 1 The apparent rate constants κ_{app} of different cycles for all samples

Catalyst	κ_{app} (min^{-1})				
Sample (h)	1st	2nd	3rd	4th	5th
5	2.94	0.68	0.59	0.3	0.24
10	3.00	0.96	0.6	0.32	0.28
24	3.04	1.10	0.76	0.38	0.3
36	3.10	1.24	0.76	0.43	0.32

excess KBH_4, its concentration can be assumed to be a constant during the reaction. Therefore, a pseudo first-order kinetic equation can be applied to evaluate the catalytic rate. The kinetic equation of the reduction can be written as follows:

$$\frac{dC}{dt} = \kappa_{app} C_t \; or \; \ln\left(\frac{C_t}{C_0}\right) = \ln\left(\frac{A_t}{A_0}\right) = -\kappa_{app} t \qquad (1)$$

where the ratios of 4-NP concentrations C_t (at time t) to its initial value C_0 ($t = 0$) were directly given by the relative intensity of the respective absorbance A_t/A_0, κ_{app} corresponds to the apparent rate constant. The apparent rate constant, κ_{app}, was calculated as 3.10 min^{-1} for the reduction of 4-NP of the prepared Ag-decorated SnO_2 microsphere at 150 °C for 36 h (Fig. 6b). In order to further assess the catalytic performance of the Ag-decorated SnO_2, all the samples prepared for different hydrothermal time were carried out to catalytic reduction of the 4-NP. The UV–Vis absorption spectra of the reduction are shown in Additional file 1: Figure S2–S5, and the corresponding plots of $\ln(C_t/C_0)$ versus time are shown in Fig. 7. It is clear that almost 100% of 4-NP can be reduced within 1 min of the first cycle. With the increase of cycle times, the time is longer. Nevertheless, over 80% of 4-NP can be reused within 8 min. It can be observed that $\ln(C_t/C_0)$ values show good linear correlation with the reaction time for all catalysts, indicating that the reduction follows a first-order reaction law. The calculated apparent rate constants κ_{app} of different cycles for all samples are shown in Table 1.

As shown in Fig. 7 and Table 1, the apparent rate constants (κ_{app}) increase with the extension of the hydrothermal time and decrease with the cycle times, especially for the first and second cycles. The decreases of rate constant may due to the peeling off and coagulation of Ag NPs from the microsphere during the centrifugation. In order to prove the stability of the sample prepared in the work, the separated catalyst (prepared for 36 h) was reused to catalytic reduction of 4-NP for more than five cycles. The time-dependent UV–Vis absorption spectra of the sixth cycle to tenth cycle are shown in Additional file 1: Figure S6. The corresponding apparent rate constants (κ_{app}) shown in Fig. 8 show there is only a slight decrease in the κ_{app} value with the increasing of successive cycles, indicating that after the first five cycles, the catalysts are much more stable than the freshly prepared samples. This proves that the as-prepared Ag-decorated SnO_2 samples possesses good stability for the catalytic reduction of 4-NP to p-AP by KBH_4 and can be used as an alternative active and stable catalyst for the catalytic reduction of 4-NP.

Also, the FTIR spectra of the catalyst before and after five cycles and ten cycles of catalytic reduction were shown in ESI. As shown in Additional file 1: Figure S7, after five and ten cycles of catalytic reduction, the main peaks of the samples were almost the same with the as-prepared sample and this illustrates that the catalysts are very stable.

In order to compare our results with other catalysts in the literature, we evaluated the catalytic ability of Ag-decorated SnO_2 by normalizing the κ_{app} values to κ_{nor} [45, 46]. The normalized rate constant κ_{nor} ($\kappa_{nor} = \kappa_{app}/c_{cat}$, where c_{cat} is the concentration of the catalyst) is a key indicator for estimating catalytic activity. The normalized rate constants κ_{nor} were calculated to be 6.20, 0.64, and 0.54 $min^{-1}g^{-1}L$ of the first cycle, fifth cycle, and tenth cycle for the SnO_2/Ag microsphere reacted for 36 h, respectively. The comparison of κ_{nor} of the SnO_2/

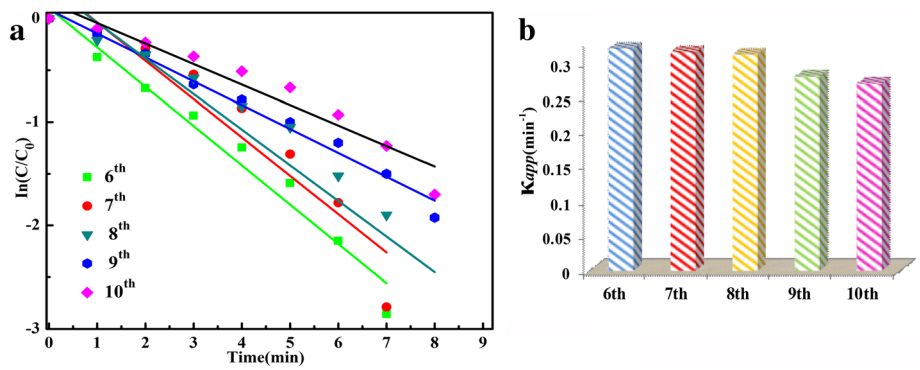

Fig. 8 a, **b** Plot of $\ln(C_t/C_0)$ versus reaction time of the sixth to tenth cycles for the 36 h sample

Table 2 Comparison of normalized rate (κ_{nor}) of different catalysts for the reduction of 4-NP (at room temperature)

Catalyst	κ_{app} (min^{-1})	κ_{nor} ($min^{-1}g^{-1}L$)	Ref.	Issue
Au/TiO_2	0.17	0.34	[47]	J Catal
Core-shell Ag@Pt	0.15	0.92	[48]	J Catal
Ag/KCC-1	0.6	9	[49]	J Catal
Au/PMMA	0.43	3.25	[50]	J Mol Catal A-Chem
meso-Co_3O_4	~0.018	0.23	[51]	Appl. Catal. B: Environ
$Co@SiO_2$	0.82	4.08	[52]	Inorg. Chem.
rGO/Fe_3O_4/Au	0.69	0.52	[53]	Phys. Chem. Chem. Phys
AgNPs/GR-G3.0PAMAM	1.30	0.78	[54]	J Mol Catal A-Chem
Ag	0.3	1.30	[55]	J. Phys. Chem. C
Ag	0.20	0.29	[56]	Catal Sci Technol
Ag	0.13	0.007	[57]	J Alloy Compd
SnO_2	0.05	0.04	[58]	Mater. Lett.
SnO_2/Ag (36 h)—1st	3.10	6.20	This work	–
SnO_2/Ag (36 h)—5th	0.32	0.64	This work	–
SnO_2/Ag (36 h)—10th	0.28	0.54	This work	–
Pure SnO_2	1.24	2.48	This work	–
Pure Ag	1.16	2.32	This work	–

Ag (36 h) and other catalysts in literature are shown in Table 2. From Table 2, it is obvious that the normalized apparent rate constant κ_{nor} of the sample in this work is much higher than that of some reported catalysts in literature [47–58], such as core-shell Ag@Pt (0.92 $min^{-1}g^{-1}L$), AgNPs/GR-G3.0PAMAM (0.78 $min^{-1}g^{-1}L$), rGO/Fe_3O_4/Au (0.52 $min^{-1}g^{-1}L$). Moreover, for the fifth and tenth cycles, the calculated κ_{nor} (0.64 and 0.54 $min^{-1}g^{-1}L$) are even higher than these catalysts [51–58]. All these results illustrate that the prepared SnO_2/Ag microsphere can be taken as a potential efficient catalyst for the reduction of 4-NP.

Based on the previous results and the traditional theory about the catalytic reduction of p-NP by noble metals, the formation mechanism and the origin of the excellent catalytic efficiency of hierarchal Ag-decorated SnO_2 microsphere were speculated and the schematic is shown in Figs. 9 and 10. In the facile one-pot hydrothermal method, the Ag and SnO_2 NPs were formed simultaneously in the solution and the freshly born surfaces are inclined to bond with each other. With the increase in hydrothermal time, the SnO_2 nanoparticles assembled into nanosheets [59] and Ag nanoparticles dispersed in the microsphere. During the catalytic reduction, the Ag nanoparticles start the catalytic reduction by relaying electrons from the donor BH_4^- to the acceptor 4-NP on the adsorption sites of the samples, which was accelerated by the intimate bond between SnO_2 and Ag NP. Moreover, the dispersed Ag NPs in the microsphere can avoid agglomeration during the catalytic reaction owing to the steric hindrance effect. Furthermore, the synergistic effect of Ag NPs and SnO_2 nanosheets co-contribute to the excellent catalytic activity of Ag-decorated SnO_2 composites. In order to verify the assumption, pure SnO_2 and Ag NPs were synthesized by the similar procedures without the addition of $AgNO_3$ and Na_2SnO_3, respectively, and then served for the catalytic reduction of 4-NP. The time-dependent UV–Vis spectra and corresponding plots of $\ln(C_t/C_0)$ versus time for SnO_2 and Ag NPs are shown in Additional file 1: Figure S8 and Figure S9. It can be observed the reduction also follows a first-order reaction law. The rate constant (κ_{app}) values calculated from the slope of the linear region were found to be 1.24 min^{-1},

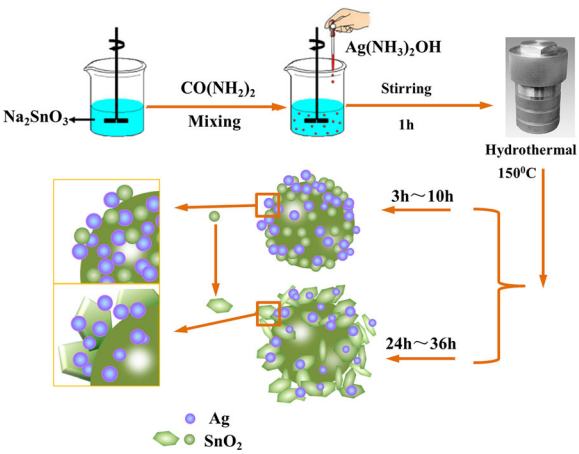

Fig. 9 Schematic illustrations of the synthesis of Ag-decorated SnO_2 microsphere

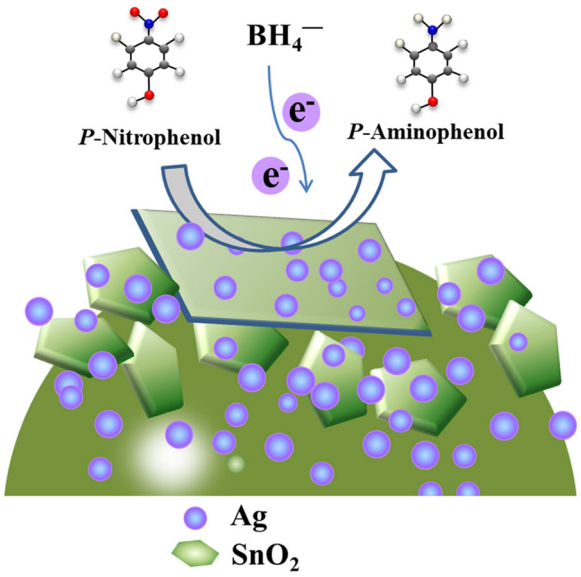

Fig. 10 Schematic illustrations of the catalytic reduction of 4-NP to 4-AP over Ag-decorated SnO_2 microsphere

and 1.16 min^{-1} for SnO_2 and Ag, which is lower than that of SnO_2/Ag. So the excellent catalytic activity of SnO_2/Ag may arise from the synergistic effect between Ag nanoparticles and SnO_2 nanosheets. However, the accurate mechanism needs to be further explored.

Conclusions

In conclusion, hierarchal Ag-decorated SnO_2 microsphere with uniform Ag nanoparticles and SnO_2 nanosheets has been successfully prepared by a facile one-pot method. The catalysts prepared by this simple but effective method exhibit excellent catalytic performance for the reduction of 4-NP to 4-AP with κ_{nor} of 6.20 $min^{-1}g^{-1}L$. Furthermore, the catalyst can sustain high catalytic performance after the first five cycles and could be expected to act as high-efficiency catalysts for the reduction of 4-NP. Moreover, we believe this method can be used as a new strategy to prepare other metal particle-modified semiconductor composites.

Additional file

Additional file 1: Figure S1. XRD patterns of the SnO_2/Ag prepared at different temperatures and different contents of mole ratio of Ag. **Figure S2.** Time-dependent UV–Vis spectra for first to fifth cycles for the sample with 5 h hydrothermal time. **Figure S3.** Time-dependent UV–Vis spectra for first to fifth cycles for the sample with 10-h hydrothermal time. **Figure S4.** Time-dependent UV–Vis spectra for first to fifth cycles for the sample with 24-h hydrothermal time. **Figure S5.** Time-dependent UV–Vis spectra for first to fifth cycles for the sample with 36-h hydrothermal time. **Figure S6.** Time-dependent UV–Vis spectra for sixth to tenth cycles for the sample with 36-h hydrothermal time. **Figure S7.** FTIR spectrum of SnO_2/Ag microsphere after different catalytic cycles. **Figure S8.** Time-dependent UV–Vis spectra for pure SnO_2 and Ag NPs. **Figure S9.** Plot of $\ln(C_t/C_0)$ versus reaction time of the pure SnO_2 and Ag. (DOCX 2159 kb)

Acknowledgements
This work was financially supported by the NSF of China (nos. 51502155, 51572152, and 21373122), the Research Project of Hubei Provincial Department of Education (no. D20151203), and the NSF of Hubei Province of China (nos. 2011CDA118 and D20151203).

Authors' Contributions
HM and LCK fabricated the samples. ZZW carried out the structural and catalytic characterization. QXQ analyzed the data. All authors read and approved the final manuscript.

Competing Interests
The authors declare that they have no competing interests.

Publisher's Note

Received: 2 March 2017 Accepted: 19 June 2017
Published online: 30 June 2017

References

1. Wang Y, Zhao ZT, Sun YJ, Li P, Ji J, Chen Y, Zhang W, Hu J (2017) Fabrication and gas sensing properties of Au-loaded SnO_2 composite nanoparticles for highly sensitive hydrogen detection. Sensors Actuators B Chem 240:664–673
2. Yuan JJ, Chen CH, Hao Y, Zhang XK, Zou B, Agrawal R, Wang C, Yu HJ, Zhu XR, Yu Y, Xiong ZZ, Luo Y, Li HX, Xie YM (2017) SnO_2/polypyrrole hollow spheres with improved cycle stability as lithium-ion battery anodes. J Alloys Compd 691:34–39
3. Fan CM, Peng Y, Zhu Q, Lin L, Wang RX, Xu AW (2013) Synproportionation reaction for the fabrication of Sn^{2+} self-doped SnO_{2-x} nanocrystals with tunable band structure and highly efficient visible light photocatalytic activity. J Phys Chem C 117:24157–24166
4. Ansari SA, Khan MM, Ansari MO, Lee J, Cho MH (2013) Biogenic synthesis, photocatalytic, and photoelectrochemical performance of Ag–ZnO nanocomposite. J Phys Chem C 117:27023–27030
5. Zhao Z, Tan H, Lv Y, Zhou LY, Song Y (2014) Reduced TiO_2 rutile nano rods with well-defined facets and their visible-light photocatalytic activity. Chem Commun 50:2755–2757
6. Saravanan R, Karthikeya N, Gupta VK, Thirumal E, Narayanan V (2013) Visible light induced degradation of methylene blue using CeO_2/V_2O_5 and CeO_2/CuO catalysts. Mat Sci Eng C-Mater 33:2235–2244
7. Kochuveedu ST, Jang YH, Kim DH (2013) A study on the mechanism for the interaction of light with noble metal-metal oxide semiconductor nanostructures for various photophysical applications. Chem Soc Rev 42: 8467–8493
8. Khan MM, Ansari SA, Ansari MO, Min BK, Lee J, Cho MH (2014) Biogenic fabrication of Au@CeO_2 nanocomposite with enhanced visible light activity. J Phys Chem C 118:9477–9484
9. Ansari SA, Khan MM, Lee J, Cho MH (2014) Highly visible light active Ag@ ZnO nanocomposites synthesized by gel-combustion route. J Ind Eng Chem 20:1602–1607
10. Lin Z, Li N, Chen Z, Fu P (2017) The effect of Ni doping concentration on the gas sensing properties of Ni doped SnO_2. Sensor Actuat B-Chem 239: 501–510
11. Liu Y, Jiao Y, Yin B, Zhang S, Qu FY (2013) Hierarchical semiconductor oxide photo catalyst: a case of the SnO_2 microflower. Nano-Micro Lett 5:234–241
12. Liu Y, Jiao Y, Zhang ZL, Qu FY, Umar A, Wu X (2014) Hierarchical SnO_2 nanostructures made of intermingled ultrathin nanosheets for environmental remediation, smart gas sensor, and supercapacitor application. ASC Appl Mater Inte 6:2174–2184
13. Liu XJ, Pan LK, Chen TQ, Li JL, Yu K, Sun Z, Sun CQ (2013) Visible light photocatalytic degradation of methylene blue by SnO_2 quantum dots prepared via microwave-assisted method. Catal Sci Technol 3:1805–1809
14. Qiao XQ, Hu FC, Hou DF, Li DS (2016) Preparation and characterization of SnO_2/Ag hollow microsphere via a convenient hydrothermal route. J Nanosci Nanotechno 16:4115–4119
15. Zhu QL, Li J, Xu Q (2013) Immobilizing metal nanoparticles to metal-organic frameworks with size and location control for optimizing catalytic performance. J Am Chem Socl 35:10210–10213

16. Wu B, Kuang Y, Zhang X, Chen J (2011) Noble metal nanoparticles/carbon nanotubes nanohybrids: synthesis and applications. Nano Today 6:75–90
17. Qiao XQ, Hu FC, Tian FY, Hou DF, Li DS (2016) Equilibrium and kinetic studies on MB adsorption by ultrathin 2D MoS_2 nanosheets. RSC Adv 6: 11631–11636
18. Qiao XQ, Hu FC, Hou DF, Li DS (2016) PEG assisted hydrothermal synthesis of hierarchical MoS_2 microspheres with excellent adsorption behavior. Mater Lett 169:241–245
19. Tan WL, Bakar NHHA, Bakar MA (2015) Catalytic reduction of p-nitrophenol using chitosan stabilized copper nanoparticles. Catal Lett 145:1626–1633
20. Dervin S, Dionysiou DD, Pillai SC (2016) 2D nanostructures for water purification: graphene and beyond. Nanoscale 8:15115–15131
21. Chen D, Ray AK (1998) Photodegradation kinetics of 4-nitrophenol in TiO_2 suspension. Water Res 32:3223–3234
22. Zhang B, Li F, Wu T, Sun DJ, Li YJ (2015) Adsorption of p-nitrophenol from aqueous solutions using nanographite oxide. Colliod Surf A 464:78–88
23. Yu TY, Zeng J, Lim B, Xia YN (2010) Aqueous-phase synthesis of Pt/CeO_2 hybrid nanostructures and their catalytic properties. Adv Mater 22:5188–519
24. Jin Z, Xiao M, Bao Z, Wang P, Wang J (2012) A general approach to mesoporous metal oxide microspheres loaded with noble metal nanoparticles. Angew Chem Int Ed 51:6406–6410
25. Deka P, Deka RC, Bharali P (2014) In situ generated copper nanoparticle catalyzed reduction of 4-nitrophenol. New J Chem 38:1789–1793
26. Qiao XQ, Zhang ZW, Tian FY, Hou DF, Tian ZF, Li DS, Zhang QC(2017) Enhanced catalytic reduction of p-nitrophenol on ultrathin MoS_2 nanosheets decorated noble-metal nanoparticles. Cryst Growth Des 17 (6):3538–3547
27. Xu GW, Wu Y, Dong WW, Zhao J, Wu XQ, Li DS, Zhang QC (2017) A multifunctional Tb-MOF for highly discriminative sensing of Eu^{3+}/Dy^{3+} and as a catalyst support of Ag nanoparticles, Small 13:1602996(1-8)
28. Zhao P, Feng X, Huang D, Yang G, Astruc D (2015) Basic concepts and recent advances in nitrophenol reduction by gold-and other transition metal nanoparticles. Coord Chem Rev 287:114–136
29. Lu P, Campbell CT, Xia Y (2013) A sinter-resistant catalytic system fabricated by maneuvering the selectivity of SiO_2 deposition onto TiO_2 surface versus Pt nanoparticle surface. Nano Lett 13:4957–4962
30. Liu P, Zhao M (2009) Silver nanoparticle supported on halloysite nanotubes catalyzed reduction of 4-nitrophenol (4-NP). Appl Surf Sci 255:3989–3993
31. Du Y, Chen HL, Chen RZ, Xu NP (2004) Synthesis of p-aminophenol from p-nitrophenol over nano-sized nickel catalysts. Appl Catal A Gen 277:259–264
32. Saha S, Pal A, Kundu S, Basu S, Pal T (2010) Photochemical green synthesis of calcium-alginate-stabilized Ag and Au nanoparticles and their catalytic application to 4-nitrophenol reduction. Langmuir 26:2885–2893
33. Zhou L, Zhou MH, Hu ZX, Bi ZH, Serrano KG (2014) Chemically modified graphite felt as an efficient cathode in electro-Fenton for p-nitrophenol degradation. Electrochim Acta 140:376–383
34. Nischala K, Rao TN, Hebalkar N (2011) Silica–silver core–shell particles for antibacterial textile application. Colloids Surf B 82:203–208
35. Matsushima S, Teraoka Y, Miura N, Yamazoe N (1988) Electronic interaction between metal additives and tin dioxide in tin dioxide-based gas sensors. Jpn J Appl Phys Part 1 27:1798–1802
36. Cao X, Cao L, Yao W, Ye X (1996) Structural characterization of Pd-doped SnO_2 thin films using XPS. Surf Interface Anal 24:662–671
37. Taylor J, Merchant S, Perry D (1995) Study of the oxidation of gold-tin preforms using X-ray photoelectron spectroscopy. J Appl Phys 78:5356–5361
38. Peng WQ, Qu SC, Cong GW, Wang ZG (2006) Synthesis and structures of morphology-controlled ZnO nano- and microcrystals. Cryst Growth Des 6: 1518–1522
39. Xu CK, Xu GD, Liu YK, Zhao XL, Wang GH (2002) Preparation and characterization of SnO_2 nanorods by thermal decomposition of SnC_2O_4 precursor. Scripta Mater 46:789–794
40. Moon T, Hwang ST, Jung DR, Son DY, Kim C, Kim J, Kang M, Park B (2007) Hydroxyl-quenching effects on the photoluminescence properties of SnO_2: Eu^{3+} nanoparticles. J Phys Chem C 111:4164–4167
41. Ramgir NS, Mulla IS, Vijayamohanan KP (2005) Effect of ruO_2 in the shape selectivity of submicron-sized SnO_2 structures. J Phys Chem B 109:12297–12303
42. Ansari SA, Khan MM, Ansari MO, Lee J, Cho MH (2014) Highly photoactive SnO_2 nanostructures engineered by electrochemically active biofilm. New J Chem 38:2462–2469
43. Sing KSW, Everett DH, Haul RAW, Moscou L, Pierotti RA, Rouquerol J, Siemieniewska T (1985) Reporting physisorption data for gas/solid systems with special reference to the determination of surface-area and porosity. Pure Appl Chem 57:603–619
44. Peng YS, Leng WG, Dong B, Ge R, Duan HD, Gao YA (2015) Bottom-up preparation of gold nanoparticle-mesoporous silica composite nanotubes as a catalyst for the reduction of 4-nitrophenol. Chin J Cata 36:1117–1123
45. Konar S, Kalita H, Puvvada N, Tantubay S, Kr Mahto M, Biswas S, Pathak A (2016) Shape-dependent catalytic activity of CuO nanostructures. J Catal 336:11–22
46. Chen HH, Yuan M, Tao S, Chen GW (2017) Oxygen vacancy enhanced catalytic activity of reduced Co3O4 towards p-nitrophenol reduction. Appl Catal B: Environ 209:648–656
47. Li BX, Hao YG, Shao XK, Tang HD, Wang T, Zhu JB, Yan SL (2015) Synthesis of hierarchically porous metal oxides and Au/TiO_2 nanohybrids for photodegradation of organic dye and catalytic reduction of 4-nitrophenol. J Catal 329:368–378
48. Ma Y, Wu XY, Zhang GK (2017) Core-shell Ag@Pt nanoparticles supported on sepiolite nanofibers for the catalytic reduction of nitrophenols in water: enhanced catalytic performance and DFT study. J Catal 205:262–270
49. Dong ZP, Le XD, Li XL, Zhang W, Dong CX, Ma JT (2014) Silver nanoparticles immobilized on fibrous nano-silica as highly efficient and recyclable heterogeneous catalyst for reduction of 4-nitrophenol and 2-nitroaniline. J Catal 158–159:129–135
50. Kuroda K, Ishida T, Haruta M (2009) Reduction of 4-nitrophenol to 4-aminophenol over Au nanoparticles deposited on PMMA. J Mol Catal A-Chem 298:7–11
51. Mogudi BM, Ncube P, Meijboom R (2016) Catalytic activity of mesoporous cobalt oxides with controlled porosity and crystallite sizes: evaluation using the reduction of 4-nitrophenol. Appl Catal B: Environ 198:74–82
52. Yan N, Zhao Z, Li Y, Wang F, Zhong H, Chen QW (2014) Synthesis of novel two-phase Co@SiO_2 nanorattles with high catalytic activity. Inorg Chem 53:9073–9079
53. Wang Y, Li H, Zhang JJ, Yan XY, Chen ZX (2016) Fe_3O_4 and Au nanoparticles dispersed on the graphene support as a highly active catalyst toward the reduction of 4-nitrophenol. Phys Chem Chem Phys 18:615–623
54. Rajesh R, Venkatesan R (2012) Encapsulation of silver nanoparticles into graphite grafted with hyperbranched poly(amidoamine) dendrimer and their catalytic activity towards reduction of nitro aromatics. J Mol Catal A-Chem 359:88–96
55. Rashid MH, Mandal TK (2007) Synthesis and catalytic application of nanostructured silver dendrites. J Phys Chem C 111:16750–16760
56. Chang GH, Luo YL, Lu WB, Qin XY, Asiri MA, Al YAO, Sun XP (2012) Ag nanoparticles decorated polyaniline nanofibers: synthesis, characterization, and applications toward catalytic reduction of 4-nitrophenol and electrochemical detection of H_2O_2 and glucose. Catal Sci Technol 2:800–806
57. Jiang D, Xie JM, Chen M, Li D, Zhu JJ, Qin HR (2011) Facile route to silver submicron-sized particles and their catalytic activity towards 4-nitrophenol reduction. J Alloy Compd 509:1975–1979
58. Bhattacharjee A, Ahmaruzzaman M (2015) A green approach for the synthesis of SnO_2 nanoparticles and its application in the reduction of p-nitrophenol. Mater Lett 157:260–264
59. Wang C, Du GH, Ståhl K, Huang HX, Zhong YJ, Jiang JZ (2012) Ultrathin SnO_2 nanosheets: oriented attachment mechanism, nonstoichiometric defects, and enhanced lithium-ion battery performances. J Phys Chem C 116:4000–4011